Syracuse University

Research Oral Document

Modeling bidisperse confluent tissues and the search for physical mechanisms of cell sorting

Preeti Sahu

Advisors:

Prof. Lisa Manning

Prof. Cristina Marchetti

Prof Jennifer Schwarz

Post Doc Mentor:

Dr. Daniel Sussman

Submission Date : December 5, 2017

Contents

Abstract

Cell sorting occurs when a heterogeneous cell mixture segregates into distinct regions and is thought to play an important role in development and disease. Although sorting has been well-studied using simulations that model cells as rigid particles, recent discoveries suggest that in confluent tissues where there are no gaps or overlaps between cells, both fluid-solid transitions and surface tension are strongly influenced by cell shapes and topologies. Even experimentally, robust cell sorting is observed in 2D co-culture of breast carcinoma and non-malignant cell lines. Therefore, we seek to analyze the behavior of cell sorting in a confluent model of tissues. Using a 2D Self-Propelled Voronoi (SPV) model, we investigate the role of disparity in cell shape and size in cell sorting for bidisperse mixtures. We find minimal sorting when cell shapes differ, but perhaps more enhanced sorting when cell sizes differ. For the latter finding, we propose additional tests to better determine the robustness of our results. We will also discuss how our results differ from bidisperse mixtures of particles and implications for biology.

1 Introduction

Cell sorting is the process whereby a mixture of two randomly mixed cell populations segregates into distinct domains homogeneous in cell types. Pattern formation by segregation of cell types is a crucial process during disease proliferation and embryonic development. In fact, a long-standing question in embryology is how cells organize themselves into coherent patterns in the absence of pre-existing or external sources of spatial information [9]. To understand this process better, numerous experiments on heterogeneous mixtures have been carried out *in-vitro* [12]. Let us try to understand cell sorting terminology by referring to some *in-vitro* cell sorting experiments that were done using cell types of different histological origins. In most of these experiments, cells from two different embryonic origins sort into structures where cells of one type form a layer surrounding those of the other type (as shown in figure:1–a). For example, in a mixture of malignant and normal breast cells (figure:1–b), the normal cells form a continuous outer layer surrounding an internal mass of malignant breast cells. Cell sorting is also used in the formation of organoids from stem cells[44]. Therefore, understanding the physical mechanisms that drive co-culture segregation can help us understand the process of embryogenesis and organ development and to devise better methods for tissue engineering.

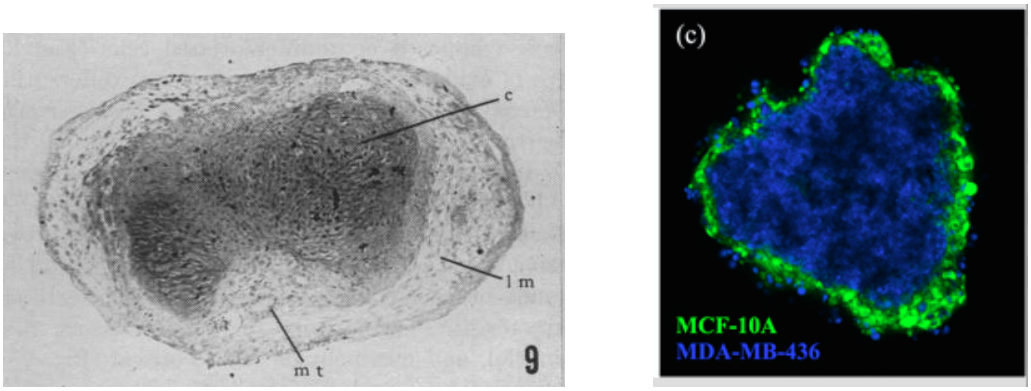

(a) (b)

Figure 1: (a) Formation of cartilage and loose mesenchyme from a mixed aggregate of dissociated cells [12] Abbbreviations: c : cartilage; Im : loose mesenchyme; (b) MCF-10A (green: normal breast epithelial cells) encloses MDAMB-436 (blue: motile-invasive cancer cell line)[24]

Cell sorting also plays a crucial role in cancer physics. Cancer is a collective phenomenon. Hence, it is important to investigate how tumour boundaries are stably maintained until metastasis occurs, enabling cells to leave the tumour and infiltrate other parts of the body. These metastatic cells seem to be hindered by two mechanical mechanisms: blocking and jamming. Blocking refers to an external steric barrier which cells cannot pass, while jamming describes a rigidity transition caused by mutual steric hindrance of the tumour cells [18]. Tumor heterogeneities might allow some parts of the tumor to fluidize while others remain rigid. Understanding sorting in such mixtures might explain what stabilizes the boundary between carcinoma and normal cells and also help answer -*what forces prevent malignant cells from exiting a solid tumor?* [18]. Understanding this will be major leap in cancer physics. It can help us predict the collective tissue property based on the mechanical properties of individual cells from minimally invasive clinical samples and therefore come up with more powerful and accurate bio-markers that forecast cancer invasiveness.

Existing hypotheses do not yet provide a complete picture

As cell sorting is such an important process in developmental biology, many cell sorting mechanisms have been proposed. One of the first ideas to explain the way in which patterns such as stripes, spots and spirals may arise naturally out of a homogeneous, uniform state [13] is based on morphogens. For a system which is originally homogeneous, these morphogens react together and diffuse through a tissue. This spatial organization of morphogens drives the formation of chemical pre-patterning. This is known as the '**Reaction-Diffusion**' view of morphogenesis asserting that mechanical rearrangements of cells are driven by pre-existing chemical pattern:

$$\texttt{chemistry} \Rightarrow \texttt{geometry} \Rightarrow \texttt{mechanics}$$

This theory based on the reaction-diffusion assumption has been widely applied for several pattern formation events although not many morphogens have been identified as yet. Models based on this theory are generally very sensitive to variations in parameters. But in real embryonic development, for example, pattern formation

is a very stable process and is hence expected to be resistant to small perturbations in the patterning process [11].

The elusive nature of morphogens and experimental evidence that cells exert traction forces on their environment [2] were the impetus for the initial development of a mechanochemical modelling approach. To contextualize the idea- many embryonic cells generate substantial contractile forces as they spread and crawl. These forces mechanically deform each cell's local environment, and the resulting distortions can alter subsequent cell movements by convection and the mechanisms of contact guidance and haptotaxis (a directional cell movement or growth in response to adhesive substrates) ([14]). The approach takes into account the cumulative effects of these cell-generated forces and shows how they can lead to the formation of regular large-scale patterns in cell populations. In contrast to the 'chemical prepattern' view, the **Murray-Oster mechanochemical model** of pattern formation is based on the view that the tissue geometry is the result of cell mechanics, and need not be specified by a detailed chemical prepattern:

$$\texttt{chemistry} \Rightarrow \texttt{mechanics} \Rightarrow \texttt{geometry}$$

Another theoretical approach, which is more relevant to this project, is the sorting model. While there are several versions of this model, they all assume that tissues behave like liquids. Thus mixtures of two different kinds, sort in a fashion similar to segregation of two immiscible liquids. For example, when oil sorts from water, an oil droplet has a surface tension associated with it that governs the way it grows by further coalescing with other droplets. The different versions of sorting models, which I will be describing next, basically try to explain what is contributing to this surface tension in the context of tissue co-cultures. The first among all is the **Differential Adhesion Hypothesis (DAH)** which was proposed by Steinberg in 1963 ([3]). The idea of DAH is that tissue behave like immiscible liquids composed of motile cells that rearrange in order to minimize their interfacial tension. It additionally assumes that difference in surface tension of tissues are caused by differences in cell-cell adhesion. This hypothesis also has experimental support later as TST was found to be directly proportional to cadherin (a type of cell adhesion molecule) expression [24].

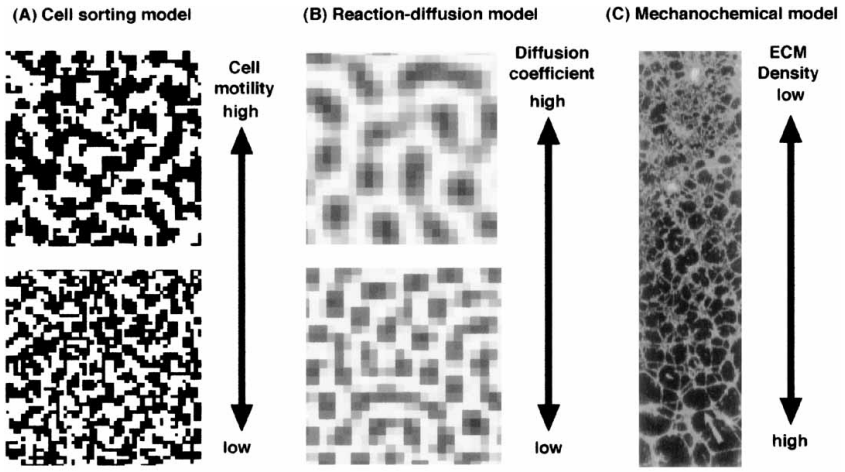

Figure 2: Prediction of the pattern change during differentiation of fibroblasts into chondrocytes according to the three kinds of models. A: shows a result of a cell sorting simulation (Mochizuki et al., 1996) when cell motility was altered. B: shows the pattern predicted by the reaction-diffusion model (Kondo and Asai, 1995) when the diffusion coefficient was altered. C: is the pattern formation in vitro (adapted from Vernon *et al.*, 1992) with varied ECM properties. Computer simulation of the mechanochemical model was unsuccessful because of its complexity. The mechanochemical model was ruled out as a mechanism for this differentiation process. [15]

Although DAH is one of the most accepted hypotheses in the field, it alone is not sufficient to explain sorting behaviour in germ-layer organization in zebrafish [21]. Harris [5] and later Brodland [6], put forth the second candidate as actomyosin contractility. According to **differential surface contraction hypothesis (DSCH)**, cells with higher contractility have lower tissue surface tension. A slightly different version of this theory is the DITH- **differential interfacial tension hypothesis**. DITH is essentially complementary to DAH. It is based on the same physical principles, but introduces cortical contractility as the key force that must be balanced to reach equilibrium. Experimental evidence for this hypothesis was found for gastrulating zebrafish embryos[7]. Mertz *et al.*, [26] also found that DITH explains the surface tension better than DAH. They compared a simple physical model of cohesive colonies as adherent contractile disks. The model captures the essential observations and suggests that the apparent surface tension in the large-colony limit is driven by acto-myosin contractility.

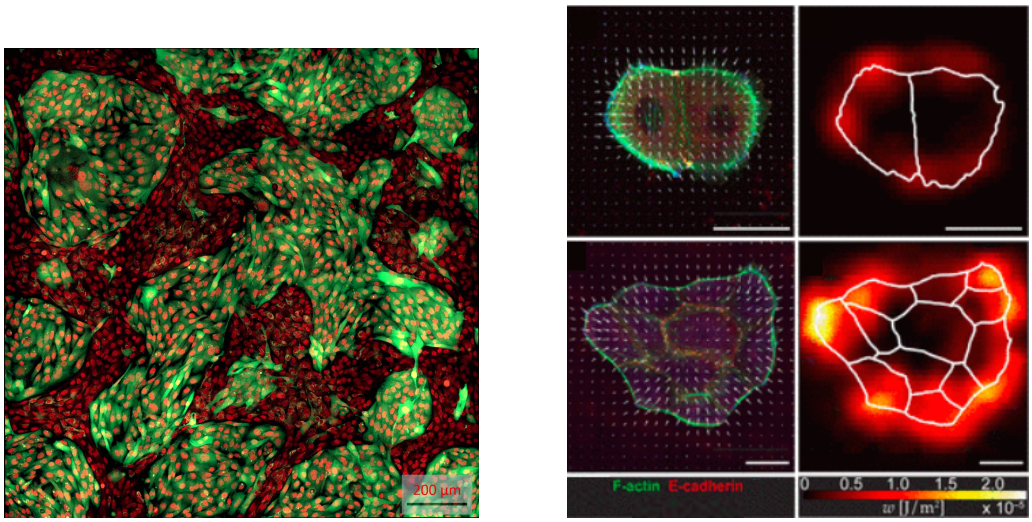

(a) (b)

Figure 3: (a) Domain formation in a bimixture of healthy breast cells and metastatic breast cells- Käs group : The green tagged cells are MDA-MB 231 (human breast cancer cell line) and the rest are MCF 10a (normal human mammary gland cell line) (b) Localization of traction force at the boundary of a colony of cells[26]. Scale bars represent 50 m.

Both of the above hypotheses assume that all cells inside a cluster are mechanistically identical and that either adhesion or contractility at a cellular level contributes in some fashion to the macroscopic TST (tissue surface tension). But there are several evidences that suggest that cells respond differently when at the boundary versus when they are in bulk i.e they *mechanically polarize*[22] at the boundary. To understand this effect better, let us consider the smallest system - a doublet of cells. Since both the cells are at boundary, according to this theory, Cadherin-mediated adhesion, reorganizes the actomysin network to intensify contractility along the external edge of a doublet and down-regulate along the internal interface. Extending this idea to larger aggregates, one might expect the contractility to be much lower inside the aggregate than on the periphery. It has been recently shown that this effect at the periphery is similar to the effect of having an increased effective adhesion [25]. The effective adhesion according to this hypothesis, and hence the name- **extended DAH**, has orders of magnitude higher contribution from contractility than from adhesion. This suggests that TST is dominated by the contribution of mechanical polarization rather than adhesion.

The sorting model is based on the idea that tissue behave like liquids, in that they tend to minimize their surface tension. Hence, an agglomerate will always be a spherical droplet and in the presence of another agglomerate, it fuses to form another spherical droplet. But some biological tissues also have solid-like properties. For example, coalescence experiments in cancer cell lines show an arrested fusion that persists over 24 hours [4]. For these solid-like aggregates, an arrest is expected when the tissue surface energy precisely balances the resistance to plastic deformations in the solid. Also, the agglomerates formed by carcinoma cells either in co-cultures (figure:3–a) or homogeneous suspensions, are not spherical in shape [24]. They have protrusions and some even have holes. Therefore, one should look beyond these theories to explain tissue dynamics.

Several computational approaches to simulate tissues

As theories evolved, computational expertise also grew hand in hand in an attempt to replicate experimental observations via simulations. Morphogen associated simulations had numerous parameters and the outcomes were heavily dependent on these parameters. Mechanochemical models, on the other hand, are difficult to simulate as the Extra-Cellular Matrix (ECM :surrounding environment of a tissue in-vivo) is complex to model. So simulations that required a minimal set of parameters and yet captured some basic features of cell sorting were developed. Particle models are simpler to simulate and so one of the techniques used to study tissues is a self-propelled particle(SPP) model [38, 27]. These models have nicely incorporated motility and persistence into cellular motion and have interesting cluster formations that reproduce density-dependent clustering observed in living cells very well. But much of the tissue dynamics *in-vivo* occurs while maintaining confluence (spatial density is unity); which is why space-filled models will be preferred over particle models here.

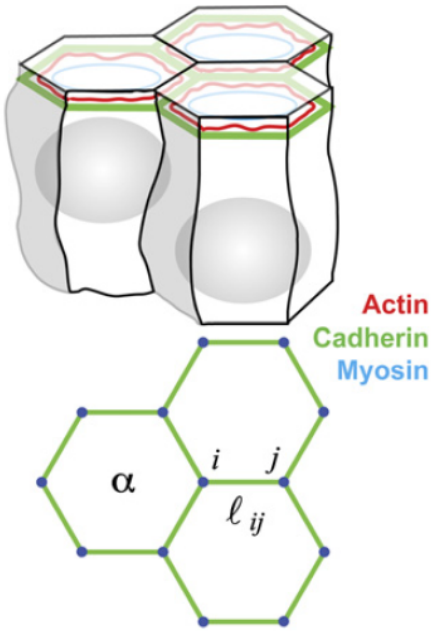

(a)

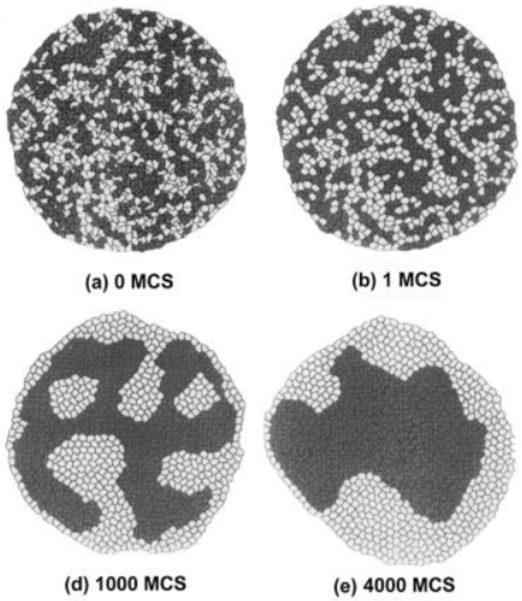

(b)

Figure 4: (a)-a apicolaterally enriched adhesion molecule Cadherin and components of the actin cytoskeleton (a)-b Cell packing geometry defined by the network of adherens junctions [31] This network is described by a vertex model with N_C polygonal cells numbered by $a = 1...N_C$ and N_V vertices, numbered $i = 1$. N_V at which cell edges meet. (b) Simulation of cell sorting using CPM: There are three cell types, "light", "dark", and "medium", $\tau \subset \{l, d, M\}$. Surface energies have been assigned values of J(d, d) =2, J(d,l) =11, J(l,l)=14, and J(d,M) =J(I,M) =16.

Let us glance through some of the relevant computational and theoretical advancements made by the community in simulating confluent tissues. For tessellating a space, space-filling models generally use Potts model, vertex and voronoi tessallations (VT). A **Cellular Potts Model** (CPM) [28] is a stochastic model where cells in a monolayer are represented as regions in figure 4–b on a lattice. The dynamic evolution calculated with a Monte Carlo algorithm is based on a Hamiltonian that includes interfacial tension, area conservation and active motility.

$$H_{CPM} = \sum_{\sigma} \lambda_v (V_\sigma - V_\sigma^T)^2 + \sum_{(\mathbf{x},\mathbf{x}')} J(\tau, \tau')(1 - \delta_{\sigma,\sigma'}) \tag{1}$$

The first summation runs over all cells and penalizes the deviation of the cell's volume (V_σ) from a prescribed target volume (V_σ^T) with a coefficient λ_v. The second term sums the adhesion energies (J) of all pairs at the cell boundaries where the cells occupying adjacent lattice site pairs $(\mathbf{x}, \mathbf{x}')$ are different i.e. $\sigma_{\mathbf{x}} \neq \sigma_{\mathbf{x}'}$. As J is typically positive for heterotypic contacts i.e. $\tau \neq \tau'$, cells tend to minimize their surface area with other cells or the medium, making the adhesion term equivalent to surface tension. Regarding the ease of implementation, a single cell in the CPM clearly has a lot more than 1 degree of freedom, hence larger systems will be slower to simulate.

The **active vertex model** has a similar energy functional except with explicit dependence on the perimeter up to second order. Each cell, as shown in Figure 4–a tries to minimize this energy functional.

$$H_{AVM} = \sum_{\alpha} \frac{K}{2}(A_\alpha - A_\alpha^{(0)})^2 + \sum_{<i,j>} \Lambda_{ij} l_{ij} + \sum_{\alpha} \frac{\Gamma_\alpha}{2} L_\alpha^2 \tag{2}$$

The energy function describes forces due to cell elasticity, actin-myosin bundles, and adhesion molecules. The first term describes an area elasticity with elastic coefficients K, for which A_α is the area of cell α and $A_\alpha^{(0)}$ is the preferred area, which is determined by cell height and cell volume. The second term describes line tensions Λ_{ij} at junctions between individual cells. Here, l_{ij} denotes the length of the junction linking vertices i and j and the sum over $< i, j >$ is over all bonds. Line tensions can be reduced by increasing cell-cell adhesion or reducing actin-myosin contractility. The third term describes the contractility of the cell perimeter L_α by a coefficient Λ_α, which could reflect, for example, the mechanics and contractility of the actin-myosin ring. The degrees of freedom of a single cell here are its vertices.

Self-propelled Voronoi model, on the other hand, uses the same energy functional as 2 but with different degrees of freedom. The 2D version of this is explained in detail in the following section. As the degrees of freedom for a single cell here is just its own center, it is much faster than all of the above models. SPV implementation is easier and one can easily incorporate activity by adding propulsion to cell centers. Homogeneously growing, confluent monolayers are very accurately described by Voronoi tessallations of their nuclei [29].

Recently, a unique kind of rigidity transition was discovered in a 2D vertex model [36]. A dimensionless parameter called the shape index (the ratio of perimeter to the square root of area) is a way of quantifying whether the cell is roundish or elongated. It has a very low value if it is roundish as it has the lowest perimeter. Shape index is important because, in experiments, mesenchymal (fluid-like) cells are very elongated whereas epithilial (solid-like) cells are more roundish [1]. A transition from a fluid-like to a rigid-like tissue was observed at a critical value of shape target index 3.81. Below this critical value of target shape index, the tissue behaves like a rigid elastic solid. This rigidity vanishes when the shape target index exceeds 3.81 and the tissue fluidizes. Since this result was obtained without any activity in the system, this transition was also explored in the SPV model with activity. As found by Bi *et al.* [20], a fluid to solid transition also occurs when the average shape parameter is 3.81. For more solid-like cells, it remains 3.81; whereas for liquid-like cells, it strives to attain its target shape index. Bi et al also demonstrated that the phase boundary depends on the activity. The phase diagram is shown in Figure 5–a.

Goal

Given the biological phenomenon of cell sorting, we will construct a bidisperse mixture of two distinct cell types in an SPV model and look for mechanisms for cell sorting. Given the hypotheses described above involving surface tension, we will focus on the fluid region of the SPV rigidity phase diagram. In other words, each cell type independently will be in the fluid region. We will then explore whether or not two distinct cell types sort (demix) depending on the parameters. This is our goal.

More specifically, we ask the following questions: *Hypothesis 1* - Is shape anisotropy a mechanism for cell sorting? *Hypothesis 2* - Is inhomogeneity in size a mechanism cell sorting? To answer these questions, we present the model and methods used, then present results, followed by a discussion of the implications of our results.

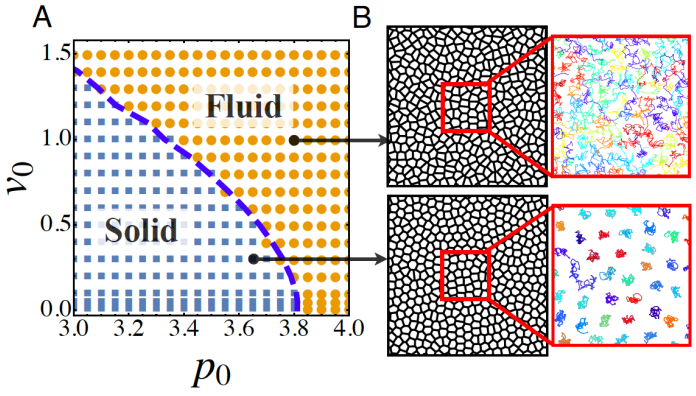

(a)

Figure 5: (a) Glassy phase diagram for confluent tissues [20] : Yellow dots are fluid like and are elongated as depicted by their shape parameter.

2 Methods and Models

We simulate the confluent tissue mixtures using a recently developed Self Propelled Voronoi (SPV) model for confluent tissues. This model merges vertex model (eq2) and self propelled particle models [35]. In this model each cell is defined by lines defined by the lines bisecting the segments connecting the center of the cell ($\vec{r}_l$) to its neighbors, resulting into a polygon of of area A_i and perimeter P_i. The mechanical cell-cell interactions are described by the shape energy E used in the VM. Each cell, with area A_i and perimeter P_i, pays a quadratic penalty to deviate from its preferred area and perimeter (A_0 & P_0 respectively). Deviations can be made costly by increasing the area stiffness K_a or cortex stiffness K_p. Energy Functional for the j^{th} cell-

$$E_j = K_a(A_j - A_0)^2 + K_p(P_j - P_0)^2$$

It can be non-dimensionalised by dividing the entire equation by $K_a A_0^2$ -

$$e_j = (a_j - 1)^2 + \frac{1}{r}(p_j - p_0)^2$$

where $p_0 = P_0/\sqrt{A_0}$, is the target shape index; $a_j = A_j/A_0$ and $p_j = P_j/\sqrt{A_j}$ are the non-dimensionalised area and perimeter respectively; $r = K_p/(K_a A_0)$ is a dimensionless parameter controlling the ratio between both the stiffnesses. If adhesion is stronger than contractility for a cell, it will have a higher perimeter to maximize it's interface with neighbouring cells. For the same reason, a cell with dominant contractile term, will be more roundish. Hence p_0 is higher for highly adhesive cells and lower for roundish cells. Cells exert force on each other as they want to minimize the overall mechanical energy. This leads to a force on each cell given by $\mathbf{F}_i = -\nabla_i E$.

We then add a self propulsion force F_0 that represents cell motility and polarization. The equation of motion for a single cell takes the form-

$$\dot{\mathbf{r}}_i = \mu \mathbf{F}_i + v_0 \hat{\mathbf{n}}_i$$

where $E = \sum E_j$ and is a non-local effective mechanical force experienced by the i^{th} cell. Here $v_0 = \mu F_0$ is the self propulsion speed of individual cells, $\hat{n}_i = (sin\theta_i, cos\theta_i)$ is the direction of polarization and μ is the mobility (inverse of drag force due to interactions with the fluid and the substrate). The polarization angle dynamics is entirely controlled by white rotational noise $\eta_i(t)$ as-

$$\dot{\theta}_i = \sqrt{2D_r}\eta_i(t)$$

$$\langle \eta_i(t)\eta_j(t')\rangle = \delta_{ij}\delta(t - t')$$

where η_i is the white noise process with mean zero and variance D_r. In the absence of mechanical interactions, an isolated cell performs a persistent random walk with a long time effective diffusion rate of $v_0^2/(2D_r\mu)$ as in SPP models. For most of our simulations $D_r = 1$ implying a persistence timescale of $1/D_r = 1$ unit. The simulations use over-damped Euler integration method. After each time step, a new Voronoi tessellation is generated based on the updated cell positions. The cell shapes are determined in the process and the exchange of cell neighbors occurs naturally through T1 topological transitions.

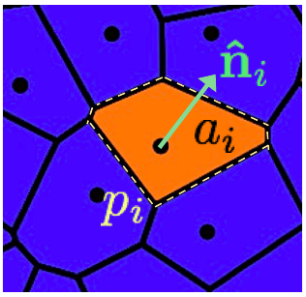

Figure 6: A Sample SPV cell: the yellow dotted line at the periphery represents perimeter p_0; orange coloured space is the area a_0

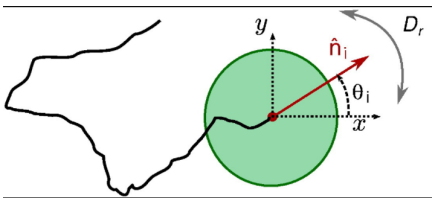

Figure 7: Dynamics of an active particle [38]; $\mathbf{n}_i$ represents the director

2.1 Binary Mixtures

To verify our first hypothesis, we mix equal number of elongated cells and roundish cells (target shape index as defined in the previous section) together. For the second hypothesis, we study mixtures with different cell size ratios. Since its is a 2D system, cell areas are tweaked to change cell size. The minimal pattern formation seen in the first model is quantified with respect to a reference state. We chose to create a VT and tag half of the cells, chosen randomly, as one type and the rest as the other type. This reference state is named **RVT- R**andom **V**oronoi **T**esallation for the rest of the report.

2.2 Quantification measures

Mean Square Displacement (MSD)- is the displacement of a particle in a given interval of time t. Here the position-$\mathbf{x}$ is with respect to the instantaneous center of mass of the system (as we are not interested in the ballistic motion of the entire system). Averaging is done over all particles, ensembles and time when in steady state.

$$MSD(t) \equiv < (\mathbf{x}(t) - \mathbf{x}(0))^2 > \tag{3}$$

Self-diffusivity D_s, is the diffusion constant with which a particle typically diffuses in the tissue.

$$D_s = \lim_{t\to\infty} \frac{MSD(t)}{4t} \tag{4}$$

To have an estimate of interactions, it is sometimes useful to compare it to the *bare* or non-interacting diffusion constant D_0. For a non-interacting but self propelled particle, with velocity v_0 and persistence time $1/D_r$, system one can easily calculate $D_0 = v_0^2/D_r$

$$D'_{eff} = \frac{D_s}{D_0} \tag{5}$$

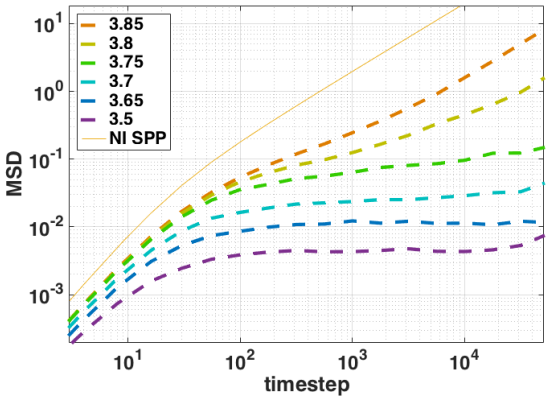

Figure 8: The dashed lines are the MSD for different homogeneous systems ranging from high $p_0 = 3.86$ (yellow) to low $p_0 = 3.5$ (purple). The solid yellow line denotes the MSD for non-interacting SPP model. For this system, $K_a = 1$ and $v_0 = 0.1$.

We need a good measure for quantifying demixing. The measures we are using are broadly operating at two different lengthscales- 1) single cell size and 2) cluster size. A very simple measure at small-scale level would be to look at the neighbour list of every individual particle and compute the proportion of homotypic neighbours. This quantity then averaged over the entire tessallation is defined as the **Demixing Parameter -DP**.

For a completely mixed scenario, the DP is 0.5, whereas for a completely sorted out mixture, the DP is maximum = 1 (in the limit of infinite systemsize). There are some cases, like - striped domains, where it drops below 0.5 as well.

$$DP_i = \frac{homotypic\ \ neighbors}{total\ \ neighbors} \tag{6}$$

This is very closely related to measures that are used by other groups to quantify cell sorting-heterotypic boundary length (HBL)[10], number of homotypic contacts divided by heterotypic contacts[40] and relative Length of Heterotypic Interface (rLHI)[33] which is the sum of all heterotypic interfaces compared to the perimeter of the maximally sorted state. Because of their local nature, in cases where there are numerous small clusters, these parameters fails to capture information about domain formation, size and shape.

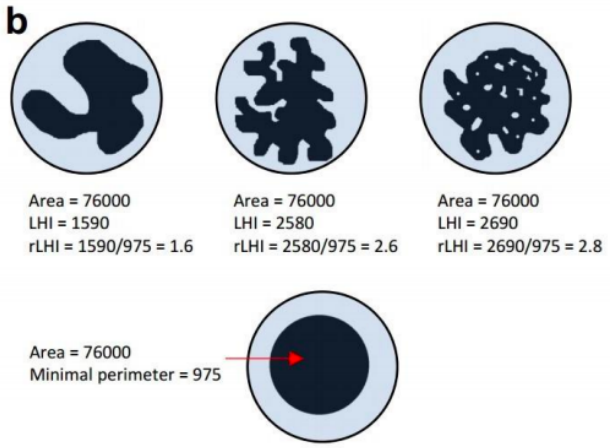

Figure 9: rLHI-The diagrams represent symbolized aggregates (light blue circles) in which the labelled cells occupy the same area (black surface), but with different distributions. [33]

Recalling from phase separation in immiscible liquids, a liquid like domain, inside another liquid prefers to be spherical as it is the most energetically favourable configuration. But as our mixtures are more complex-viscoelastic entities, we may not get such compact cluster formation given the accessible region of simulation time. Therefore, having a quantification for an effective radius and asphericity can prove to be a good measure of validity of different theories too.

Radius of Gyration Tensor- $\Re$, defined below, can help us understand this asphericity better.

$$\Re = \begin{bmatrix} \Re_{xx} & \Re_{xy} \\ \Re_{xy} & \Re_{yy} \end{bmatrix} \tag{7}$$

Where each component is defined as-

$$\Re_{xy} = \frac{1}{N}\sum_{i=1}^{N}(x_i - X_{cm})(y_i - Y_{cm})$$

Diagonalizing $\Re$ gives us with two eigenvalues in 2D- (λ_1, λ_2). The trace is **Radius of Gyration -**R_g which tells us about the effective radius of a cluster. It is the root mean square deviation of each member from the center of mass of the cluster. It can be computed as-

$$R_g^2 =< r_i^2 > - < R_{cm} >^2 = \lambda_1 + \lambda_2 \tag{8}$$

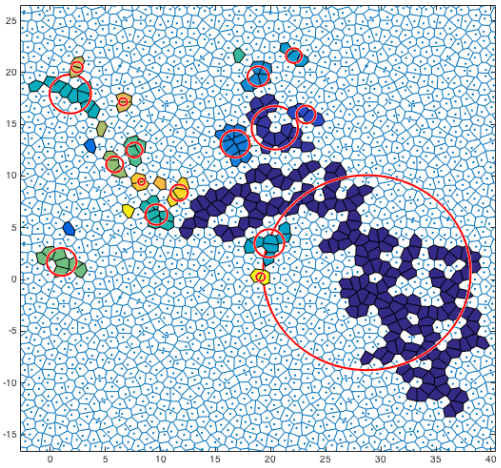

Figure 10: Radius of gyration of fractal like clusters formed by highly elongated cells, when mixed with roundish cells.

We have already seen very compact domain formation in cell-cell co-cultures in figure:3–a. **Fractal Dimension -**D_f is a great tool to understand how compact a cluster is. String-like clusters can be differentiated from compact clusters using D_f [42].

$$N \propto R_g^{D_f} \tag{9}$$

where D_f is the fractal dimension. Hence a D_f of 1, indicates string-like cluster whereas a D_f of 2, indicates a compact 2-dimensional cluster like a disc.

For systems with periodicity a length scale can be extracted using the **structure factor - S**

$$S(\mathbf{k}) = \frac{1}{N}\left\langle \sum_{i,j} e^{i\mathbf{k}\cdot\mathbf{r}_{ij}} \right\rangle \tag{10}$$

where r_{ij} is the vector between all the pairs of particles in the system. Since there is no angular dependence for isotropic systems, I deal with the radial distribution in k-space of S mostly. S(k) is the fourier transform of **Pair Correlation function - g**(r). g(r) accounts for the probability of finding the center of a particle a given distance from the center of another particle by normalizing by the density; thus at large values of r it goes to 1, uniform probability.

$$g(r) = \frac{1}{2\pi r N \rho_0}\sum_{i}^{N}\sum_{j}^{N}\delta(r - r_{ij}) \tag{11}$$

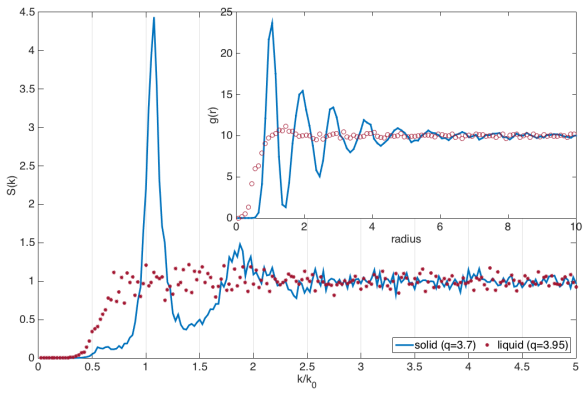

Figure 11: Structure factor for a single realization of N=1600 cells of a homogeneous system; inset- Pair correlation for the same system. The blue curves are for $p_0 = 3.7$ and the red curves are for $p_0 = 3.95$. As we can see the blue curves resemble the structure factor of hard spheres.

In a two-component mixture, there are 3 quantities one can look at- S_{AA}, S_{BB} and S_{AB}. Where first two give the structure for each type of particle in the mixture, the later gives information about correlation between different types of particles. Eventually we want to compute the characteristic length-scale in the system by computing the dominant k as per the following formula-

$$L(t) = \frac{\int_{2\pi/L}^{q_{max}} S(q,t)dq}{\int_{2\pi/L}^{q_{max}} qS(q,t)dq} \tag{12}$$

q_{max} is chosen as the maximum value of k that occurs at the end of the first peak in structure factor. Time evolution can give scaling behaviors that can help us understand the mechanism of cluster formation.

We set up the SPV code to simulate a N-particle binary mixture comprised half of Type A cells and half of Type B cells. We then set up simulations (usually a hundred different initializations) run for a variable number of timesteps as described below. For example, if we are trying to calculate DP, we try to run it long enough such that DP saturates. After the runs complete, we use the parameters we described in the previous section to analyze the properties of each individual model, after calibrating it first with the reference system wherever possible.

3 Results

3.1 Binary mixtures with two target perimeters

Previous work has identified a "coarsening instability" in the vertex model [31, 32], where some cells shrink in size and others grow. It is possible that heterogeneous p0 values exacerbate this problem. In many real heterogeneous tissues, such coarsening is not seen, so we'd like to avoid that in our model. A visual inspection of particles in this mixture indicated wide fluctuations in area. Hence we first try to find out what are the values of K_a needed to avoid spurious dynamical or coarsening features in these bidisperse mixtures.

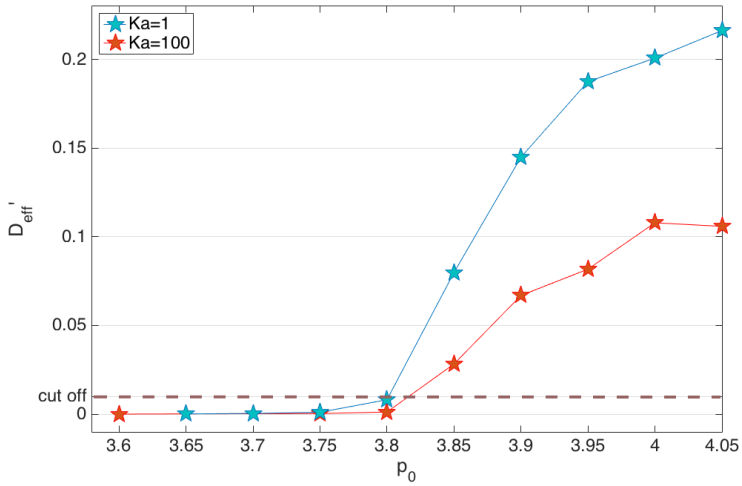

Figure 12: The graph plots effective diffusivity with respect to preferred perimeter; The Red curve is for $K_a = 100$. It is compared to the blue curve which is for the standard $K_a = 1$ case

Increasing K_a ensures that cells do not contract below their target areas to achieve a lower p_0. Figure above shows that increased area stiffness has nearly no impact on the fluidity (computed using eq 5 ,4 to compute the effective diffusivity) of systems homogeneous in p_0. So even with huge dispersity in p_0 , I now have a way to reduce the coarsening that frustrates the entire tessellation ,without compromising on fluidity of the components.

Since we're interested in finding the cause behind demixing, we need to understand what region of this multi-dimensional parameter space is useful for our objective. In other words, do we need to check all of the phase space (solid-solid, solid-fluid, fluid-fluid) or is it useful to focus only on the fluid-fluid region?

Fluidity is very crucial for demixing as cells need to move to sort. We already have an idea of fluidity from results in homogeneous mixtures [20]. But we need to understand how does the fluidity of each individual tissue type influence the fluidity of the two-component system? Since a 2-component system can have many possible compositions, we can think of this space being spanned by an average value of shape index and difference between two shape indices. Since in our case, area is constrained to be unity, average value of shape index can be unambiguously denoted by $< p_0 >= \phi_a p_{0a} + \phi_b p_{0b}$ and the difference is denoted by $\Delta = p_{0b} - p_{0a}$. We plot (in figure 13–b) the diffusivity for a fixed $< p_0 >= 3.9$. From the color plot (figure 13–b), the system is solid-like when Δ is large enough so that one of the components is solid. For all other compositions, even for the $< p_0 >$ not shown here, the mixture retains the fluidity of $< p_0 >$. This behavior was found similar for some other values of $< p_0 >$ ranging from solid-like values to liquid-like. This analysis suggests that the dynamics in solid-fluid mixtures is suppressed, so that demixing is likely very slow and

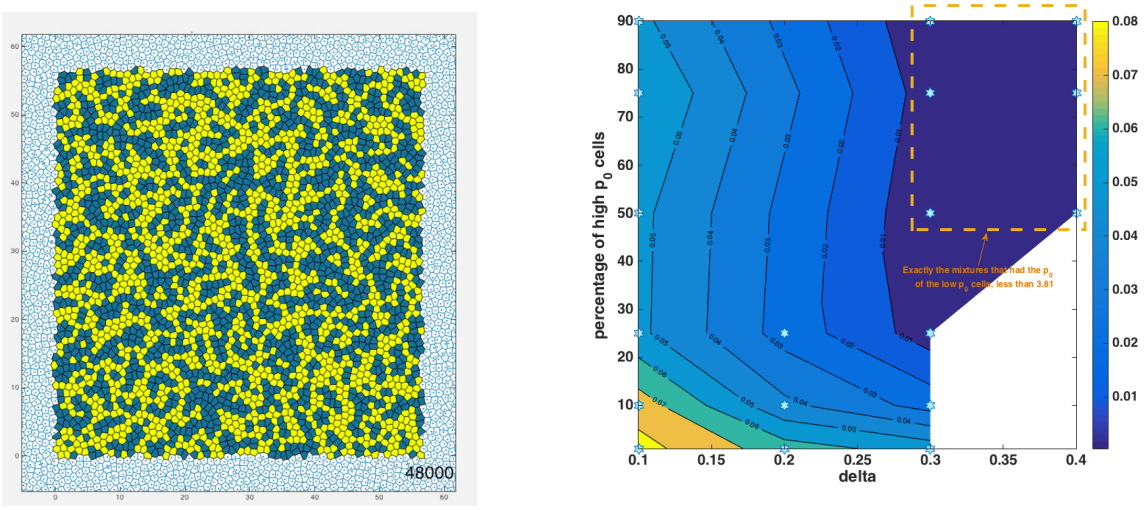

(a) (b)

Figure 13: (a) A sample of fluid-solid micro-segregation: elongated cells($p_0 = 3.95$) are mixed with roundish cells ($p_0 = 3.75$) (b) The color plot represents the effective diffusivity as a function of Δ and percentage of type A (high p_0) cells for a fixed value of $< p_0 >= 3.9$ (fluid-like). The color represents D'_{eff}; hence the darkest shade of blue is the region with diffusivity below cut-off and hence solid-like.

we already know solid-solid mixtures are not expected to sort. Hence we can now focus only on fluid-fluid mixtures. Hereafter we'll look at just 50-50 mixtures for simplicity.

Demixing Parameter

In conventional liquid-liquid mixtures, one would expect the mixture to sort if the components have different viscosities. For homogeneous systems, it is already known that in fluid regime, higher p_0 corresponds to a higher fluidity. Therefore mixing equal number of cells with two different p_0, is expected to demix. But just by looking at figure 13–a, we observe a much smaller scale segregation. Visually it is not clear if it is distinguishable from a random mix of both types. DP being a local parameter is sensitive enough to pick these small changes. To calculate DP, we use eq 6 here.

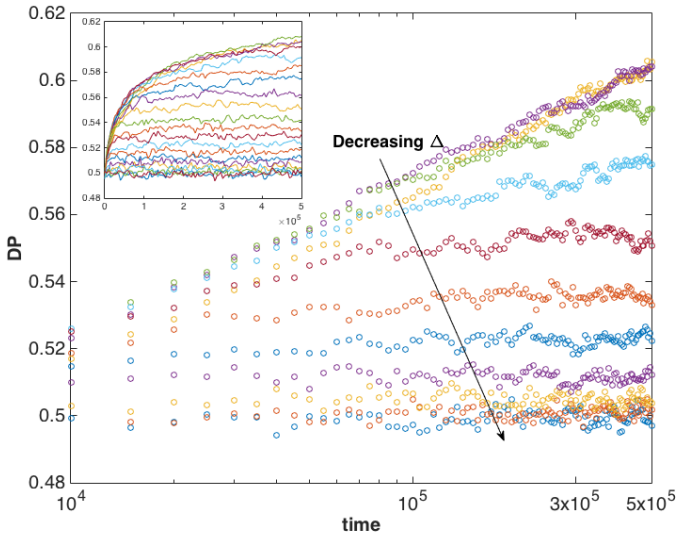

(a)

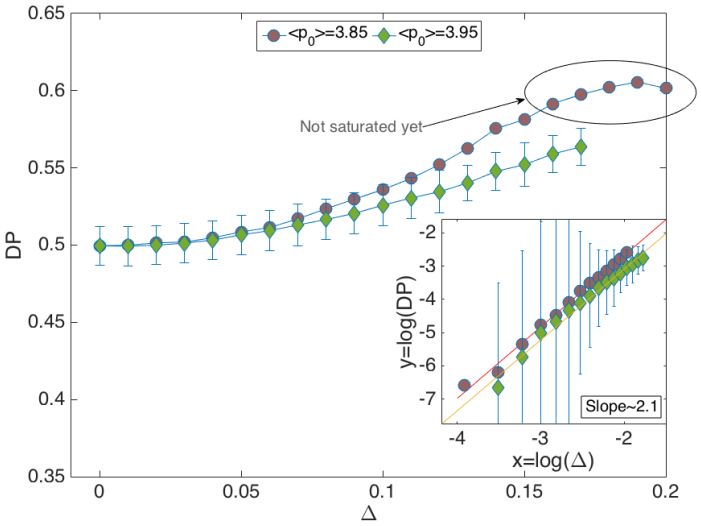

(b)

Figure 14: (a) Demixing Parameter is plotted with logarithmic time for a wide range of fluid-fluid mixtures of same $< p_0 >= 3.85$; The Δ decreases from a maximum value of 0.2 to zero, in steps of 0.02. The inset is the same graph in linear scale for both axes. (b) The steady state values of DP is plotted against Δ. Inset: a double logarithm plot of saturated steady state values of (DP-0.5) vrs Δ shows exponent to be close to 2. Points with magenta marker are for mixtures with $< p_0 >= 3.85$ and the ones with green markers are for $< p_0 >= 3.95$

Contrary to our naive expectation, they have a very minimal amount of demixing even for the largest fluid-fluid Δ. Unlike liquid mixtures, the demixing doesn't keep increasing till it becomes completely separate. Instead it saturates with a timescale that seems to depend on how far the least fluid component is from being rigid. The saturation value does seem to increase with disparity in a quadratic fashion (shown in figure 14–b).

Although the sorting is so minimal, the small clusters might still be more compact than a mixture with no bidispersity i.e RVT (as defined in sec 2.1). We expect this because in a viscoelastic mixture, local viscosity disparity might cause compactification of clusters much faster than the cluster coalescence timescale.

Since the aim is to test compactification as a function of shape disparity, the first natural quantity is the Fractal Dimension (D_f) of these clusters. We compute it by looking at the scaling laws for cluster size (to compute which I wrote a MATAB code 5.2) with respect to RoG using eq:8. For more compact clusters like a circular disc, the D_f should be the same as two whereas for extremely linear thread-like clusters will have a D_f closer to one. Hence the question we are trying to answer here is if the fractal dimension of segregated state is distinguishably lower than that of RVT. For better comparison, I choose the maximally segregated fluid-fluid mixture from figure-14–b. I compute the D_f for RVT in two different ways. Only one of the two methods is shown in the main text. The other method 5.1 requires computing the percolating cluster scaling with respect to system-size. It gives value of D_f (∼1.9) very close to already found value (∼1.89) for RVT whereas the straight forward method used here might not be as accurate(∼1.9).

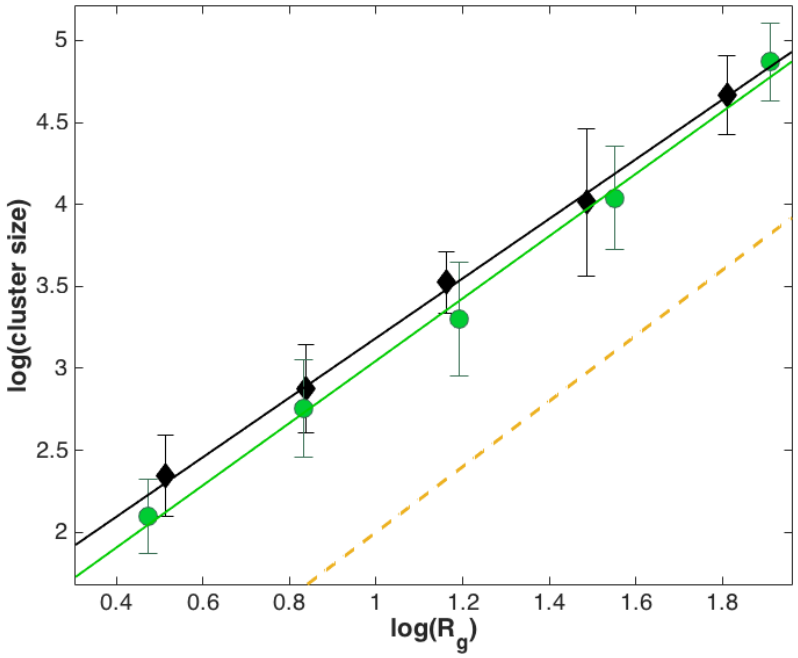

Figure 15: A double logarithm plot of cluster size vrs radius of gyration is plotted. The dashed yellow line represents an D_f of 2, green circles represent RVT and has an D_f of ~ 1.90 and black diamonds represent the mixture $< p_0 >= 3.85$ and $\Delta = 0.08$ (for a Δ higher than this the solid component enters into the solid regime). The solid lines are a linear fit to the data of respective colour. The linear region of the curve is analyzed for the slope.

The figure shows that the clusters formed are comparable to the RVT, or if anything even more branched than the RVT. This is a good indicator of the fact that this system is not segregating in a liquid-like manner, in contrast to observations made in experiments on two cell types.

3.2 Binary mixtures with two target areas

After studying the impact of shape disparity in cell sorting, we next study the effect of dispersity in area. The mixture is comprised of equal number of smaller a_0 cells and larger a_0 cells, chosen such that they average out to unity. We start from an initial configuration in which both the components are randomly mixed. For the results shown here, I have fixed the shape index s to 3.95 to mimic fluid-like cells. α here denotes the ratio of preferred a_0 s for both the types. I have also studied a small number of simulations with fixed perimeter instead of fixed target shape index but did not see much motion at few particular phase points so did not pursue it further.

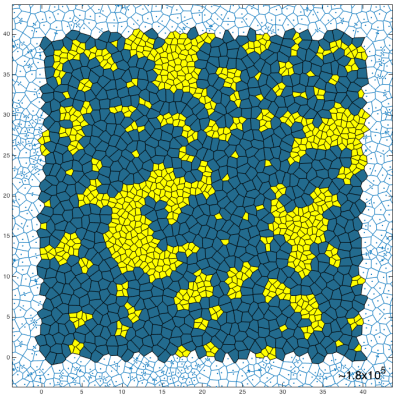

Figure 16: A typical configuration for a 50-50 mixture of cells with same shape target index but very different areas ; $\alpha = 2.5$; usual parameter values for $K_a = 1$, $v_0 = 0.1$, $D_r = 1$, dt=0.01

Demixing Parameter

We try our simplest parameter for demixing for small propulsion speeds. Looking at a snapshot of the video shows much more compact clustering than that seen in the previous model. And even in experiments the demixing is quite high. Hence we want to check if the demixing is really close to 1.

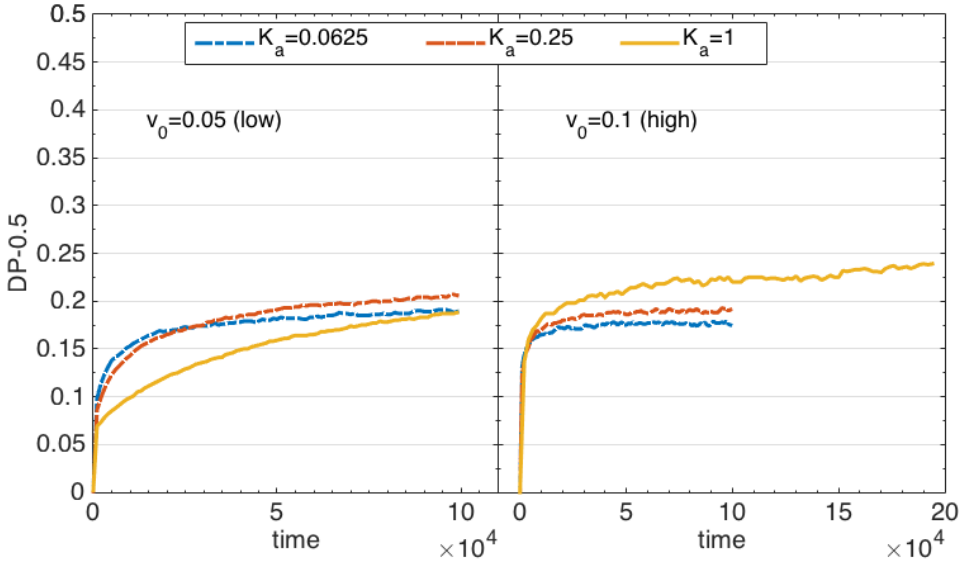

Figure 17: Increase in DP with respect to time is plotted for $\alpha = 2.5$. Different colors represent K_a values- 0.0625 (blue), 0.25 (red) and 1 (yellow). On left, the analysis is done for a lower velocity $v_0 = 0.05$ whereas on the right it is for $v_0 = 0.1$. The y-axis goes upto the maximum value possible i.e 0.5.

In the figure 17 we see that the demixing, though higher than the previous case, is not very close to 1.

To support this demixing result we try to see signatures of clustering using another measure for demixing like a lengthscale computed using the Structure factor for the clusters. We use structure factor because this is typically used in fluid simulations and one can compare the exponents found in literature directly to compare and contrast. For high clustering , we want to check if we acquire a peak very close to $k = 0$.

The figure 18 shows that we do see a huge peak very close to $k = 0$ although one needs to do ensemble averaging over several realizations to know the exact lengthscale.

The mechanism behind this segregation is not confirmed still, even though we ruled out persistence being the cause. Area stiffness and activity do seem to intensify demixing upto some extent.

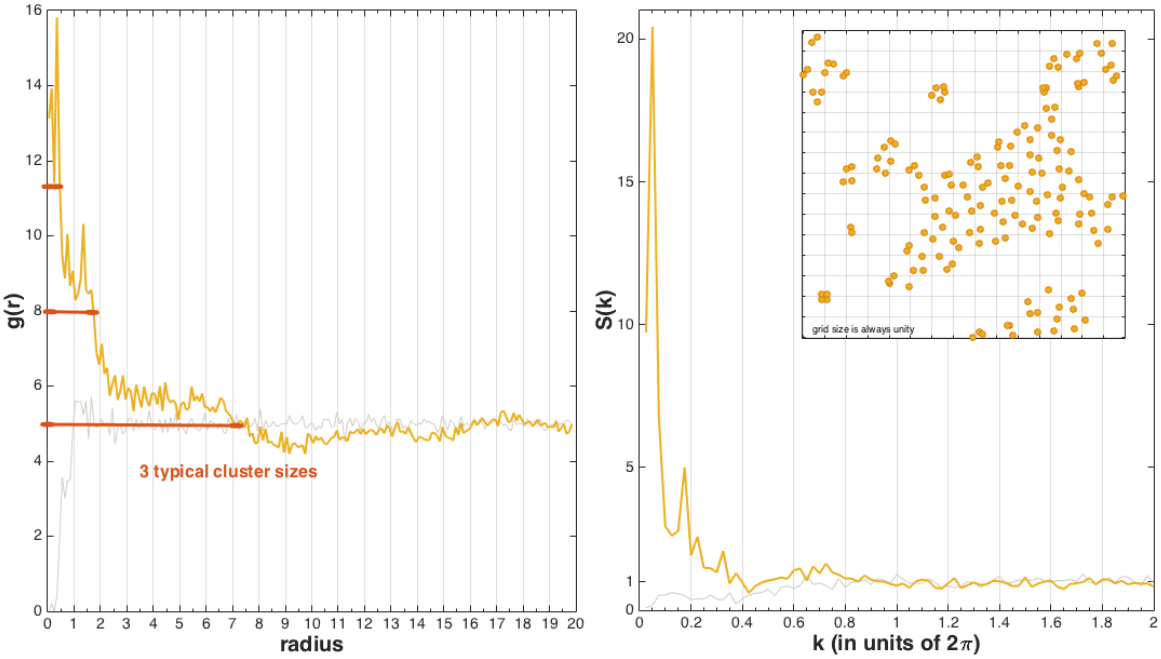

Figure 18: On left: Pair correlation function g(r) is plotted against radius. On Right- Structure factor is plotted against momentum k in units of 2π. The inset shows a portion of the data that is analyzed here. $\alpha = 2.5$; usual parameter values for $K_a = 1$, $v_0 = 0.1$, $D_r = 1$

4 Discussion

Mixing together cells of two different shapes gives rise to a very minimal amount of segregation. This micro-segregation is quantified by using several different parameters ranging from a scale as local as a single cell to more non-local measures. Local measures do indicate a small, distinguishable amount of demixing but global measures seem to indicate that the clustering is no different from the random placement of two distinct cells in a confluent tissue. One possible mechanism for these fractal-like cluster to form is to reduce the shape anisotropy by stacking elongated cells together. On the other hand, mixing two different sizes of cells together gives rise to a significant amount of demixing. Demixing increases with an increase in area disparity. More non-local measures like structure factor also give signature of clustering. We ruled out persistence as one possible mechanism, but activity and area stiffness do play a role. We plan to run more simulations to confirm this bi-disperse areas result.

Random Voronoi tessellations has been studied in great depth (some of the findings have been reproduced in the appendix 5.1) and hence, for the micro-segregated case, there is a good null model with respect to which one can compare and contrast the demixing. But for mixtures bidisperse in area, people generally use a radical Voronoi tessellation[30]. This method does Voronoi tessellations differently than the way done in this manuscript. The tessellation algorithm respects the size difference to begin with. Our current algorithm, which does not respect the size, might play a role in the cluster formation and so we propose to alter our current algorithm to use the radical Voronoi tessellation and test for robust of our two different sizes results presented here. A quick check on implementing bidispersity in vertex model can also tell us about the effect of voronoi tessellation.

Given the small amount of demixing observed in the different shapes case, let us compare our results with particle systems. If there is a segregation in the bidisperse particle systems, it is mostly because of excluded volume interactions, i.e. entropically driven segregation occurs. A mixture of long cells mixed with roundish ones, entropically favours longer cells to stack along their longer edge, as this will increase the excluded volume. 3D mixtures do show such stacking up of longer particles. Similar, is the incentive of larger cells getting attracted to larger ones[47]. But since ours is a space-filled model, this effect cannot play a role in segregation. Naively, one would not expect segregation to occur in a mixture bidisperse in area in a confluent tissue.

Looking from the perspective of pure liquids demixing from each other, the micro segregation resembles a solid-like demixing because the clusters formed are not spherical. If it were liquid, two different viscosity liquids should sort but we don't see this here. Even for the mixture bidiperse in area does not form clusters that are as compact as liquid droplets. The larger particles easily break into a cluster and the clusters are very transient. Perhaps a better comparison would be by comparing the Ostwald ripening exponent for this

process. Ostwald ripening occurs when two droplets of the disperse phase collide to form one larger and one smaller droplet. With continued collisions, the smaller droplets decrease in size until they disappear/become solubilized in the continuous phase. The large droplets continue to grow and eventually separate out. This growth exponent in 2D is found to be $(t/lnt)^{1/3}$ [46] and in 3D- $t^{1/3}$ [45].

One of our main objectives was to understand the experimentally observed robust sorting in bidisperse mixtures of malignant and healthy cells. Since we do not yet observe that in the modeling, perhaps we need to put heterotypic line tension between two different cell types explicitly into the model to achieve more compact segregation. The experiments also indicate a difference in activity between the two types. We will next explore both possibilities to continue to search for physical mechanisms for cell sorting.

5 Appendix

5.1 RVT Characterization

These are random voronoi tesallations in which half of the total number of cells in the box, are randomly chosen to be of Type A. To have a visual idea of how it actually looks, two images for RVT are put in Fig:19–a. In a mixture of two components, one of them has to percolate. Hence, since it a 50-50 bimixture and no particular component that outnumbers the other, Type A percolates in statistically half of the cases.

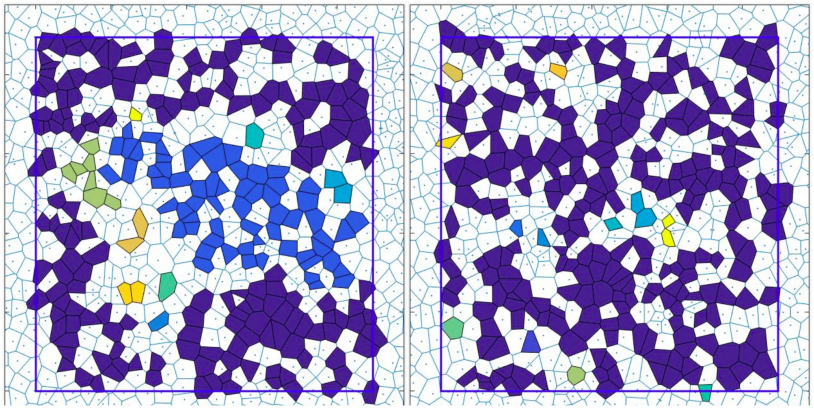

(a)

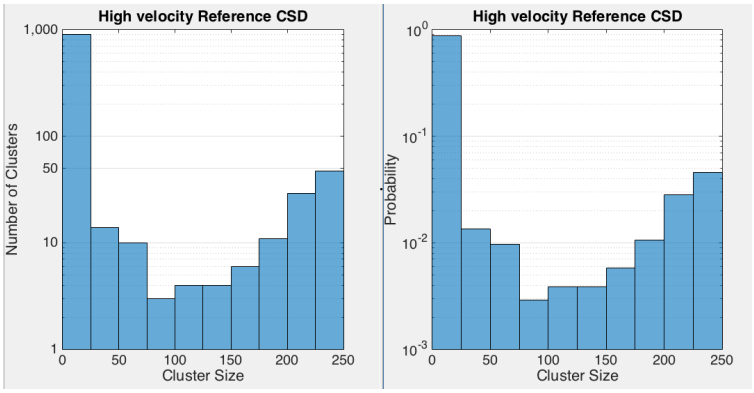

(b)

Figure 19: (a) Some samples of RVT; The colored cells are Type A and the rest inside the box are Type B. Left image is one is which Type A doesn't percolate whereas in the right one it does. The different colours just represent distinct Type A clusters. (b) The cluster size distribution (CSD) plotted in two different scales: the left one represents the raw counts whereas the right histogram bins probability ie normalized by total number of clusters. There are 100 ensembles taken into consideration for this plot. The left plot tell us that there were nearly 50 percolating Type A clusters in the entire lot.

Fractal dimension for the Reference state

It is known [39] that for RVT, the threshold ratio, for percolation, of Type A cells is 0.5. To prove the fractal nature of this threshold system let us compute its FD. One way is to look at the largest clusters and how it scales with respect to system size L. Below is a scaling for such a binary mixture.

We see that at critical ratio ie 50-50, the fractal dimension is slightly less than 2. We get 1.9 which is close to the value 1.89 as reported in ref-[41]. For a higher percentage of type A cells, I get the dimension to be 2.

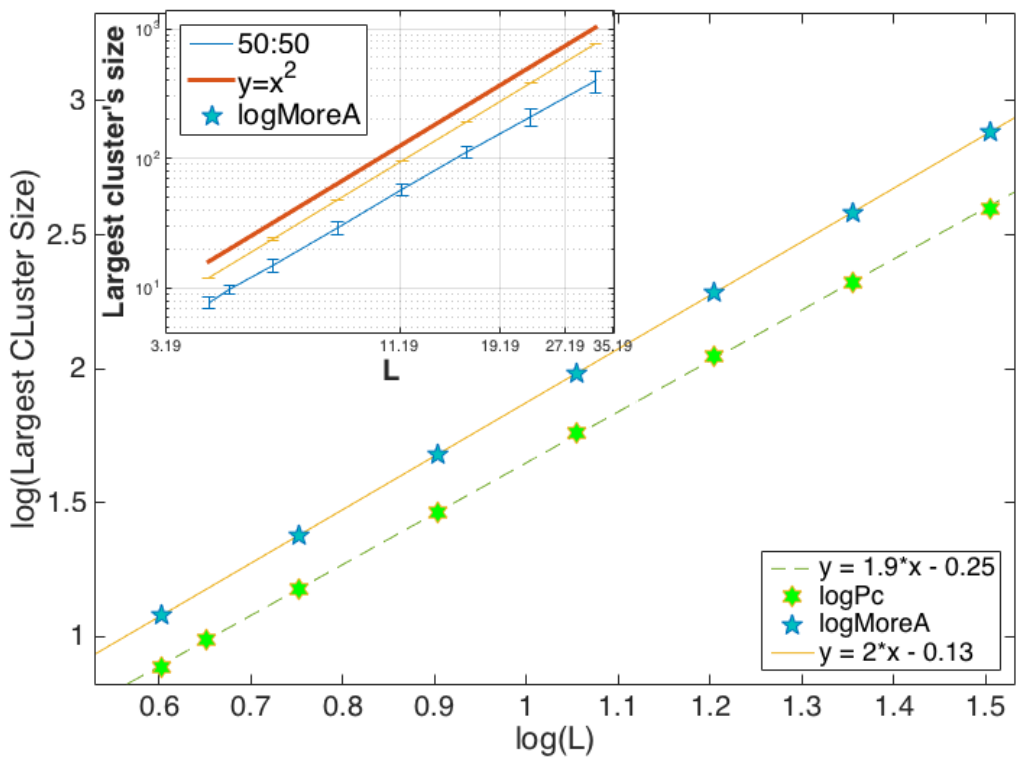

5.2 MATLAB code for cluster finding

```
cells=500;        % Total # of cells
a=sqrt(cells);  % The side length L
Na=cells/2;      % Type A cells for 50-50 bidisperse mixture
ensemno=50; % Number of realizations

% U is a cell array.
Here it is expected that a maximum of 30 clusters
%can be found. For each realization, it has information about all the
%clusters and it's members.

        U=cell(30,ensemno);
        [row, col]=size(U);
         for i=1:row
             for j=1:col
                 U{i,j}(1)=0;
             end
         end

toplot=[];

for ensm=1:ensemno

 % Let's first clear all the variables that are not needed later.
 clearvars -except cells Na toplot ensemno ensm a myXdata myYdata
 posXFiles U frame writerObj


%---Putting PBC
%-----------------
    for b =1:cells %         \_/                          \_/
    x(b,1)=myX16data{1,ensm}(1,b)-(floor(myX16data{1,ensm}(1,b)/a))*a;
    x(b,2)=myY16data{1,ensm}(1,b)-(floor(myY16data{1,ensm}(1,b)/a))*a;
    % x(b,2) is the y-coordinate of cells
    end
```

```
%--- Creating Images
%---------------------
E=x;
E(:,1)=x(:,1)+a;
W=x;
W(:,1)=x(:,1)-a;
N=x;
N(:,2)=x(:,2)+a;
S=x;
S(:,2)=x(:,2)-a;

SE(:,1)=x(:,1)+a;
SE(:,2)=x(:,2)-a;
NW(:,1)=x(:,1)-a;
NW(:,2)=x(:,2)+a;
NE=x+a;
SW=x-a;

X=[x;NE;SW;E;W;N;S;SE;NW];
%This keeps adding the new matrices at the end

[vx,vy]=voronoi(X(:,1),X(:,2));
[v,c] = voronoin(X);

%Now I have the information about the vertices of each cell in proper
%order of connectivity

%------------------ Series of inversions
%----------------------------------------

ix=[c{:}]'; % creates column vector of vertices
cellLengths = cellfun(@length, c);
cs = cumsum(cellLengths);
jy = arrayfun(@(k) nnz(cs < k), (1:cs(end))) + 1;% creates
%corresponding cell number columnlike [1,1,2,2,2,3,3,4,4,4,4,....]
S = sparse(ix, jy, true, size(v, 1), size(c, 1));
[i,j,s] = find(S); %[vertex,cell,logical]
A = full(S);
[ii, jj] = find(A);
Cinv = accumarray(ii, jj, [], @(v) {v.'});%gives me the cell array to
% know what are the cells connected to a given vertex

%------------------ Homotypic Nearest Neighbors (NN)
%--------------------------------------------------

B=zeros(Na,Na);

for i=1:Na
    for j=1:length(c{i})
        for k=1:length(Cinv{c{i}(j)})
            Inbox=Cinv{c{i}(j)}(k)-((floor(Cinv{c{i}(j)}(k)/cells)))*cells;
            if (Inbox<=Na && Inbox~=0)
 %---
                nn=Inbox;           %In box meaning inside the box
                B(i,nn)=nn ;
 %----
            end
        end
    end
end
nz_Cell_Cell_cellarray = arrayfun( @(IDX) nonzeros(B(IDX,:)), 1:size(B,1), 'Uniform', 0);

%---------Cluster-finding algorithm
%-----------------------------------
```

```
     D=[];

     clusterNo=0;
     T=zeros(1,30);

for l=1:Na

     if(ismember(l,D)==0)  %% do NOT ever use LOGICALS.. use ismmember or isdiff
             clusterNo=clusterNo+1;
             T=zeros(1,30);
             V=[];           %stores ek cluster mein kahan tak gaye
             T(1)=l;

             for n=1:50
                 n
                 T0=[];          %reset this for each tree branch so we can find the actual T

                 for p=1:length(T)
                     if(ismember(T(p),V)==0 && T(p)~=0)
                         T0=union(T0,nz_Cell_Cell_cellarray{T(p)});
                     end
                 end


         V=union(V,T);
                 T=zeros(1,30);  %reset to feed new ones

                 for q=1:length(T0)  %Check for new members only
                     if(ismember(T0(q),V)==0)
                         T(q)=T0(q);
                     end
                 end

                 U{clusterNo,ensm}=union(U{clusterNo,ensm},V');
                 % if no new member added with this iteration, stop
                 % iterating.
                  if(nnz(T)==0)
                      break
                  end

             end

             D=union(D,[U{:,ensm}]);   %  (' =transpose hai)

     end
end
```

References

[1] Castro MG, Leggett SE, Wong IY. Clustering and Jamming in Epithelial-Mesenchymal Co-Cultures. Soft matter. 2016;12(40):8327-8337. doi:10.1039/c6sm01287f.

[2] Harris, A., Wild, P., and Stopak, D. (1980). Silicone Rubber Substrata: A New Wrinkle in the Study of Cell Locomotion. Science, 208(4440), 177-179. http://www.jstor.org/stable/1683946

[3] Steinberg MS (1963) Reconstruction of tissues by dissociated cells. Some morphogenetic tissue movements and the sorting out of embryonic cells may have a commonexplanation. Science 141: 401–408.

[4] Eva-Maria Schötz, Marcos Lanio, Jared A. Talbot, M. Lisa Manning Glassy dynamics in three-dimensional embryonic tissues J. R. Soc. Interface 2013 10 20130726; DOI: 10.1098/rsif.2013.0726. Published 25 September 2013

[5] Harris A K Is Cell Sorting Caused by Differences in the Work of Intercellular Adhesion? A Critique of the Steinberg Hypothesis J. theor. Biol. (1976) 61,267-285

[6] Brodland, G. W. The Differential Interfacial Tension Hypothesis (DITH): a comprehensive theory for the self-rearrangement of embryonic cells and tissues. J. Biomech. Eng. (2002).124, 188-197.

[7] Maitre, J.-L., Berthoumieux, H., Krens, S. F. G., Salbreux, G., Julicher, F., Paluch, E. and Heisenberg, C.-P. Adhesion functions in cell sorting by mechanically coupling the cortices of adhering cells. Science (2012). 338, 253-256.

[8] Townes P and Holtfreter J Directed movements and selective adhesion of embryonic amphibian cells. J. exp. ZooI.(1955). 128, 53.

[9] William Waites, Matteo Cavaliere, Elise Cachat, Vincent Danos, Jamie A. Davies (2017) Organoid And Tissue Patterning Through Phase Separation: Use Of A Vertex Model To Relate Dynamics Of Patterning To Underlying Biophysical Parameters bioRxiv (2017) 1–18 http://biorxiv.org/content/early/2017/05/10/136366.abstract

[10] Olivier Cochet-Escartin, Tiffany Tian Locke, Winnie H Shi, Robert E Steele, Eva-Maria S Collins Forces driving cell sorting in Hydra bioRxiv (2017) https://doi.org/10.1101/142976

[11] Előd Méhes , Enys Mones, Valéria Németh, Tamás Vicsek (2012) Collective Motion of Cells Mediates Segregation and Pattern Formation in Co-Cultures PLOS ONE 7(2): e31711 https://doi.org/10.1371/journal.pone.0031711

[12] Trinkaus, J. P., and Groves, P. W. Differentiation in culture of mixed aggregates of dissociated tissue cells. PNAS, (1955). 41(10), 787–795.

[13] Turing AM The chemical basis of morphogenesis, Phil. Trans R Soc (1952) (Lond.) B237: 37–72.

[14] J. D. Murray and G. F. Oster Generation of Biological Pattern and Form; Math. Med. Biol. (1984) 1,51-75

[15] Miura, T. and Shiota, K. Extracellular matrix environment influences chondrogenic pattern formation in limb bud micromass culture: Experimental verification of theoretical models. Anat. Rec., (2000), 258: 100–107. doi:10.1002/(SICI)1097-0185(20000101)258:1¡100::AID-AR11¿3.0.CO;2-3

[16] Levental, K. R., Yu, H., Kass, L., Lakins, J. N., Egeblad, M., Erler, J. T., ... Weaver, V. M. Matrix Crosslinking Forces Tumor Progression by Enhancing Integrin signaling. Cell, (2009). 139(5), 891–906. http://doi.org/10.1016/j.cell.2009.10.027

[17] Sinkus R, Tanter M, Xydeas T, Catheline S, Bercoff J and Fink M Viscoelastic shear properties of in vivo breast lesions measured by mr elastography Magn. Reson. Imaging Magnetic Resonance Imaging 23 (2005) 159 – 165 https://doi.org/10.1016/j.mri.2004.11.060

[18] Linda Oswald, Steffen Grosser, David M Smith and Josef A Käs Jamming transitions in cancer J. Phys. D. Appl. Phys.(2017) 0022-3727 http://iopscience.iop.org/article/10.1088/1361-6463/aa8e83

[19] Anatol Fritsch, michael Höckel, tobias Kiessling, Kenechukwu David nnetu, Franziska Wetzel, mareike Zink and Käs, Josef A Are biomechanical changes necessary for tumour progression? Nature Physics 6 (2010) http://www.nature.com.libezproxy2.syr.edu/nphys/journal/v6/n10/pdf/nphys1800.pdf

[20] Dapeng Bi, Xingbo Yang, M. Cristina Marchetti and M. Lisa Manning Motility-Driven Glass and Jamming Transitions in Biological Tissues PRX 6, 021011 (2016) http://dx.doi.org/10.1103/PhysRevX.6.021011

[21] Krieg, M., Y. Arboleda-Estudillo, P.-H. Puech, J. Käfer, F. Graner, D. J. Müller, and C.-P. Heisenberg. Tensile Forces Govern Germ-Layer Organization in Zebrafish. Nature Cell Biology 2008. 10 (4): 429–36. doi:10.1038/ncb1705.

[22] Jeffrey D. Amack, M. Lisa Manning Knowing the Boundaries: Extending the Differential Adhesion Hypothesis in Embryonic Cell Sorting Science (2012) 338, 6104, 212-215 http://science.sciencemag.org/content/338/6104/212

[23] Pawlizak, Steve and Fritsch, Anatol W. and Grosser, Steffen and Ahrens, Dave and Thalheim, Tobias and Riedel, Stefanie and Kießling, Tobias R. and Oswald, Linda and Zink, Mareike and Manning, M. Lisa and Käs, Josef A. Testing the differential adhesion hypothesis across the epithelial-mesenchymal transition New J. Phys. (2015) 17, 8, 1- 10 http://iopscience.iop.org/article/10.1088/1367-2630/17/8/083049/meta

[24] Ramsey A. Foty, Malcolm S. Steinberg, The differential adhesion hypothesis: a direct evaluation, Developmental Biology, 278, 1, 2005, 255-263, ISSN 0012-1606, https://doi.org/10.1016/j.ydbio.2004.11.012. http://www.sciencedirect.com/science/article/pii/S0012160604008048

[25] Manning, M. Lisa and Foty, Ramsey A. and Steinberg, Malcolm S. and Schoetz, Eva-Maria Coaction of intercellular adhesion and cortical tension specifies tissue surface tension PNAS (2010) 107, 28, 12517–12522 http://www.pnas.org/lookup/doi/10.1073/pnas.1003743107,

[26] Mertz, Aaron F. and Banerjee, Shiladitya and Che, Yonglu and German, Guy K. and Xu, Ye and Hyland, Callen and Marchetti, M. Cristina and Horsley, Valerie and Dufresne, Eric R. PRL (2012) 108, 19, 1-5 https://link.aps.org/doi/10.1103/PhysRevLett.108.198101

[27] Xingbo Yang, M. Lisa Manning and M. Cristina Marchetti, Aggregation and segregation of confined active particles DOI: 10.1039/C4SM00927D Soft Matter, 2014, 10, 6477-6484 http://pubs.rsc.org/en/content/articlehtml/2014/sm/c4sm00927d

[28] Graner, François and Glazier, James A., Simulation of biological cell sorting using a two-dimensional extended Potts model, PhysRevLett.69.2013, doi:10.1103/PhysRevLett.69.2013 https://link.aps.org/doi/10.1103/PhysRevLett.69.2013

[29] van Drongelen, Ruben and Vazquez-Faci, Tania and Huijben, Teun A. P. M. and van der Zee, Maurijn and Idema, Timon Mechanics of epithelial tissue formation arXiv (2017) 1–11 https://arxiv.org/abs/1705.06205

[30] Song-Chuan Zhao, Stacy Sidle, Harry L. Swinney and Matthias Schroter Correlation between Voronoi volumes in disc packings EPL, 97 (2012) 34004 http://iopscience.iop.org/article/10.1209/0295-5075/97/34004/pdf

[31] Reza Farhadifar, Jens-Christian Röper, Benoit Aigouy, Suzanne Eaton, Frank Jülicher, The Influence of Cell Mechanics, Cell-Cell Interactions, and Proliferation on Epithelial Packing, Current Biology, Volume 17, Issue 24, 2007, Pages 2095-2104, ISSN 0960-9822, https://doi.org/10.1016/j.cub.2007.11.049. http://www.sciencedirect.com/science/article/pii/S0960982207023342

[32] D. B. Staple, R. Farhadifar, J. -C. Röper, B. Aigouy, S. Eaton and F. Jülicher Mechanics and remodelling of cell packings in epithelia Eur. Phys. J. E, 33 2 (2010) 117-127 arXiv:1112.5905v1 DOI: https://doi.org/10.1140/epje/i2010-10677-0

[33] Canty, Laura and Zarour, Eleyine and Kashkooli, Leily and François, Paul and Fagotto, François Sorting at embryonic boundaries requires high heterotypic interfacial tension Nat. Commun. (2017) 8,1 http://dx.doi.org/10.1038/s41467-017-00146-x

[34] Bo Li, SeanX. Sun, Coherent Motions in Confluent Cell Monolayer Sheets, In Biophysical Journal, Volume 107, Issue 7, 2014, Pages 1532-1541, ISSN 0006-3495, https://doi.org/10.1016/j.bpj.2014.08.006. (http://www.sciencedirect.com/science/article/pii/S0006349514008443)

[35] Sriram Ramaswamy The Mechanics and Statistics of Active Matter Annual Review of Condensed Matter Physics 2010 1:1, 323-345

[36] A density-independent rigidity transition in biological tissues https://www.nature.com/nphys/journal/v11/n12/pdf/nphys3471.pdf

[37] Daniel M. Sussman; cellGPU: massively parallel simulations of dynamic vertex models Computer Physics Communications, volume 219, pages 400-406, (2017)

[38] Minimal model of active colloids highlights the role of mechanical interactions in controlling the emergent behavior of active matter http://www.sciencedirect.com/science/article/pii/S1359029416300024

[39] Bollobás, Béla and Riordan, Oliver The critical probability for random Voronoi percolation in the plane is 1/2 Probab. Theory Relat. Fields (2006)136,3, 417–468 https://arxiv.org/pdf/math/0410336.pdf.

[40] Kabla, Alexandre J. Collective cell migration: leadership, invasion and segregation Journal of The Royal Society Interface (2012) 9 ,77, http://rsif.royalsocietypublishing.org/content/9/77/3268

[41] Percolation Theory https://archive.org/details/Kim_Christensen___Percolation_Theory.

[42] Evaluation of the Fractal Properties of Cluster–Cluster Aggregates http://www.tandfonline.com/doi/pdf/10.1080/02786820050204682

[43] The shape of two-dimensional percolation and Ising clusters http://iopscience.iop.org/article/10.1088/0305-4470/20/13/008/pdf

[44] Mathieu Unbekandt, Jamie A. Davies, Dissociation of embryonic kidneys followed by reaggregation allows the formation of renal tissues, In Kidney International, Volume 77, Issue 5, 2010, Pages 407-416, ISSN 0085-2538, https://doi.org/10.1038/ki.2009.482. (http://www.sciencedirect.com/science/article/pii/S0085253815542737)

[45] I.M.Lifshitz, V.V.Slyozov The kinetics of precipitation from supersaturated solid solutions In Journal of Physics and Chemistry of Solids, Volume 19, Issues 1–2, 1961, Pages 35-50, ISSN 0022-3697, https://doi.org/10.1016/0022-3697(61)90054-3

[46] A. J. Bray (2002): Theory of phase-ordering kinetics, Advances in Physics, 51:2, 481-587 http://dx.doi.org/10.1080/00018730110117433

[47] S. Aumaıtre, C. A. Kruelle, and I. Rehberg Segregation in granular matter under horizontal swirling excitation PHYSICAL REVIEW E, VOLUME 64, 041305

[48] Abdul N Malmi-Kakkada, Xin Li, Himadri S. Samanta, Sumit Sinha, D. Thirumalai Cell growth rate dictates the onset of glass to fluid-like transition and long time super-diffusion in an evolving cell colony bioRxiv 174599 http://dx.doi.org/10.1101/174599